

Article

A Facile Surface-Imprinting Strategy for Trypsin-Imprinted Polymeric Chemosensors Using Two-Step Spin-Coating

Je Wook Byeon ¹, Jin Chul Yang ¹, Chae Hwan Cho ², Seok Jin Lim ¹, Jong Pil Park ^{2,*} and Jinyoung Park ^{1,*}

¹ Department of Polymer Science & Engineering, Kyungpook National University, 80 Daehak-ro, Buk-gu, Daegu 41566, Republic of Korea

² Basic Research Laboratory, Department of Food Science and Technology, Chung-Ang University, Anseong 17546, Republic of Korea

* Correspondence: jppark@cau.ac.kr (J.P.P.); jinpark@knu.ac.kr (J.P.); Tel.: +82-31-670-4703 (J.P.P.); +82-53-950-5624 (J.P.)

Abstract: Surface imprinting used for protein recognition in functional cavities is highly effective in imprinting biomacromolecules to avoid template encapsulation during the formation of a molecularly imprinted polymer (MIP) matrix. Herein, we introduce a facile surface-imprinting method based on two-step spin-coating and photopolymerization to design highly efficient imprinted sites on polymeric films to detect trypsin (TRY). Well-distributed template imprinting is successfully achieved for maximized sensing responses by controlling the composition of functional monomers and crosslinkers in the precursor solution and the concentration of TRY in the imprinting solution. The MIP film exhibits higher sensitivity ($-841 \pm 65 \text{ Hz}/(\mu\text{g}/\text{mL})$) with a coefficient of determination of 0.970 and a higher imprinting factor of 4.5 in a 0.24 $\mu\text{g}/\text{mL}$ TRY solution compared to the nonimprinted polymer (NIP) film. Moreover, the limit of detection and limit of quantification are calculated to be 25.33 and 84.42 ng/mL, respectively. Finally, the selectivity coefficient is within the range of 3.90–6.78 for TRY against other proteins. These sensing properties are superior to those of the corresponding nonimprinted polymer matrix. Thus, the proposed facile surface-imprinting method is highly effective for protein imprinting with high sensitivity and selectivity.

Keywords: surface imprinting; molecularly imprinted polymer; photopolymerization; trypsin; spin-coating



Citation: Byeon, J.W.; Yang, J.C.; Cho, C.H.; Lim, S.J.; Park, J.P.; Park, J. A Facile Surface-Imprinting Strategy for Trypsin-Imprinted Polymeric Chemosensors Using Two-Step Spin-Coating. *Chemosensors* **2023**, *11*, 189. <https://doi.org/10.3390/chemosensors11030189>

Academic Editors: Daniele Merli and Giancarla Alberti

Received: 23 January 2023

Revised: 6 March 2023

Accepted: 10 March 2023

Published: 11 March 2023



Copyright: © 2023 by the authors. Licensee MDPI, Basel, Switzerland. This article is an open access article distributed under the terms and conditions of the Creative Commons Attribution (CC BY) license (<https://creativecommons.org/licenses/by/4.0/>).

1. Introduction

Proteolytic enzymes (proteases) are commonly used in various physiological processes such as protein absorption, digestion, tissue repair, pain relief, and cell division [1,2]. Trypsin (TRY), the most commonly used proteolytic enzyme produced and secreted by pancreatic acinar cells, plays a crucial role in digestive systems by hydrolyzing protein molecules into peptides or amino acids and activating other digestive proenzymes [3]. This enzyme has served as a biomarker for pancreatitis, pancreatic cancer, cystic fibrosis, and other diseases based on the evaluation of the TRY level in human serum [4–7]. Accordingly, various sensing platforms have been proposed to develop simple, sensitive, inexpensive, and rapid methodologies for TRY detection, such as electrochemical [8], optical [9], piezoelectric [10], and enzyme-linked immunosorbent assay [11].

The use of molecularly imprinted polymers (MIPs) as artificial biomimetic receptors for the selective detection of biomaterials is rapidly increasing owing to their excellent properties, such as high physical and chemical stability and easy and inexpensive preparation. The MIPs are fabricated mainly via the thermo-, photo-, and electrochemical polymerization of precursor mixture comprising a crosslinker, functional monomer, and target molecule (template). The removal of the template after polymerization leaves functional cavities corresponding to the size, shape, and chemical functionality of the template in the MIP matrix, enabling the selective adsorption of template molecules [12].

However, MIP-based chemosensors for protein detection have difficulties in imprinting large proteins due to the inherent characteristics of proteins, such as water-solubility, complicated conformation, and numerous functional groups [13]. Thus, the potential application of various proteins as template molecules in MIP technology is challenging because of easy protein denaturation in the presence of an organic solvent or heat during MIP fabrication. Still, novel approaches for protein imprinting, i.e., epitope imprinting [14], electropolymerization [15], and surface imprinting [16–18], have been developed to solve these issues.

A novel methodology based on epitope imprinting was reported to immobilize porcine pancreatic alpha-trypsin (PPT) [19]. Using magnetic-MIP core-shell particles, prepared with four different peptide segments as templates, the binding affinities were compared from the linear regression based on the Scatchard equation, resulting in the associated affinity between the PPT and peptide segments. Three different approaches for the surface imprinting of thin films were presented using amorphous, crystalline, and solubilized TRY as templates [20]. The solution-based polymer imprinting showed the highest specific recognition with a limit of detection (LOD) of 100 ng/mL. An electrochemically fabricated sensor with simple synthesis and precise control in the synthesis process for TRY detection has been reported. Thin bulk films electrochemically deposited on gold-coated quartz crystal (QC) electrodes showed excellent sensitivity with a limit of detection (LOD) of 70.9 ng/mL and specificity for the target protein TRY [21]. However, its preparation was successfully achieved via precise electrochemical control of polymerization, and hence electroactive monomers are essential for electropolymerization. Another reported strategy was to use a surface-imprinting system for making the MIP matrix on a protein-immobilized surface, thereby minimizing conformational changes and exposing unnecessary functional groups in proteins [22]. Thus, limitations such as slow mass transfer, heterogeneous binding sites, and template embedding associated with conventional bulk molecular imprinting could be resolved using this technique [23]. For example, surface-imprinted polymer particles immobilized on the surface of the TRY piezoelectric sensor revealed great sensitivity with an LOD of 70 ng/mL and long-term stability [10]. However, this technique required a long fabrication time and complicated procedures for template immobilization on the substrate surface. Thus, a much simpler strategy was required for easy and efficient surface imprinting for fabricating selective TRY chemosensors. As a simple method, a spin-coating strategy was reported for the preparation of bulk MIP films with controlled thickness and porosity [24]. After spin-coating a pre-polymerized MIP mixture on a substrate, the MIP films were fabricated via UV polymerization. However, this method requires some alteration for the surface imprinting of a protein template.

In this study, a simple technique for TRY surface imprinting is proposed by adopting easily accessible two-step spin-coating and photopolymerization. Using the spin-coating method, a nano-sized polymer film can be easily coated on a substrate, and the solution can be uniformly spread all over the substrate surface [25]. With this strategy, a TRY-surface-imprinted thin film could be deposited on the QC substrate through UV irradiation after spin-coating the TRY template solution on spin-coated pre-cured MIP films. To improve the detection signal through efficient imprinting, imprinting conditions are optimized by adjusting the composition of the functional monomer and crosslinker in the precursor solution and the TRY concentration in the imprinting solution. The sensing properties of poly(MAA-co-EGDMA) films coated on the QC electrodes were evaluated via microgravimetric analysis using quartz crystal microbalance (QCM). Selectivity is also evaluated using various competing proteins.

2. Materials and Methods

2.1. Materials

For the synthesis of TRY-templated MIP film, methacrylic acid (MAA) as the functional monomer and ethylene glycol dimethacrylate (EGDMA) as the crosslinker were purchased from Tokyo Chemical Industry Co. (Tokyo, Japan). TRY (M.W = 23.8 kDa,

pI = 10.1–10.5) as the template protein and 2,2-azobisisobutyronitrile (AIBN) as the photoinitiator were received from Sigma Aldrich Co. (St. Louis, MO, USA) and Daejung Chemicals (Siheung-si, South Korea), respectively. Phosphate-buffered saline (PBS) (0.01 M, pH 7.4) solution was prepared by dissolving 2.67 mM potassium chloride (Duksan Pure Chemicals Co., Ansan, South Korea), 1.8 mM potassium phosphate monobasic (Sigma Aldrich Co.), 138 mM sodium chloride (Duksan Pure Chemicals Co., South Korea), and 8 mM sodium phosphate dibasic dihydrate (Acros Organics Co., Geel, Belgium) in 1 L of distilled water. For selectivity evaluation, ovalbumin (OVA, M.W = 44.5 kDa, pI = 4.5, Acros Organics Co.), bovine serum albumin (BSA, M.W = 66.5 kDa, pI = 4.7, Roche Diagnostics GmbH Co., Mannheim, Germany), and lysozyme (LSZ, M.W = 14.3 kDa, pI = 11.35, Sigma Aldrich Co.) were used as interfering proteins. Glacial acetic acid (Duksan Pure Chemicals Co.) and sodium dodecyl sulfate (SDS, Alfa Aesar Co., Ward Hill, MA, USA) were prepared to remove the TRY template from the MIP matrix. Distilled water was acquired from a water purification system (Pure Roup 30, Pure Water Co., Namyangju, Korea), and all of the other chemicals were used without further purification.

2.2. Molecularly Imprinted Films

TRY-templated MIP films on gold substrates via spin-coating and photopolymerization were formed as follows: First, a precursor solution was prepared by mixing MAA (2 mmol), EGDMA (8 mmol), and AIBN (0.2 mmol) in a 10 mL vial using a vortex mixer for 10 min. The reaction mixture in the glass vial was sealed with a rubber stopper, and nitrogen gas (N₂) was purged for 10 min. Subsequently, the MAA/EGDMA precursor solution was pre-cured via UV irradiation for 20 s using a UV lamp ($\lambda = 370$ nm, 36 W) with the intensity of 3.5 mW/cm² at a distance of 3 cm between the mixture solution and UV lamp to afford slight crosslinking and increased viscosity. Then, 9-MHz gold-coated AT-cut quartz crystal substrates (QCs, QA-A9M AU[M], diameter = 5 mm, Seiko EG&G, Seiko Instruments Inc., Chiba, Japan) with an active gold area of 0.196 cm² were cleaned using piranha etching (H₂SO₄:H₂O₂, 3:1 (v/v)) for 20 s and UV/ozone treatment (UV/Ozone ProCleaner Plus, Bioforce Nanosciences Inc., Chicago, IL USA) for 20 min to increase the adhesion to the precursor solution. The pre-cured MIP precursor solution in the volume of 3 μ L was dispensed on the QC substrates using a micropipette. Right after spin-coating at 4000 RPM for 30 s, 5 μ L of the 0.5 mg/mL aqueous TRY imprinting solution was dynamically dispensed onto the substrate rotating at 2000 RPM and spin-coated for 60 s. A flat polydimethylsiloxane mold (PDMS, Sylgard 184, Dow Corning, Midland, MI USA), fabricated by curing a mixture of silicone elastomer base (30 g) and curing agent (3 g) at 60 °C in a vacuum pump (DOA-P704-AC, Gas Manufacturing Inc.) for 2 h, was carefully placed on the spin-coated film. After UV irradiation for 20 min, the PDMS mold was physically detached from the substrate. Imprinted protein templates on the MIP matrix were extracted by immersing them in a 10 mL mixture of SDS/acetic acid (2.5% (w/v) and 5% (v/v)) for 10 min [26]. Finally, the MIP-coated QC substrate was dipped in distilled water for 5 min and dried using N₂ gas. Likewise, NIP films were fabricated without spin-coating the TRY.

2.3. Characteristics

A field emission scanning electron microscope (FE-SEM, Hitachi S-4800) working at an accelerating voltage of 5 kV was used to identify the surface morphology and thickness of the MIP film on QC electrodes. The MIP film on the QC electrode was coated with platinum for 90 s using an ion sputter coater (E1030, Hitachi, Ltd., Tokyo, Japan) to acquire high-resolution SEM images of the MIP matrix.

To evaluate the adsorption characteristics of both MIPs and NIPs, their resonance frequency shift (Δf) was measured using a quartz crystal analyzer (QCA 922A, Seiko EG&G, Tokyo, Japan). All adsorption tests were performed after installing the TRY sensor inside a dip cell. The concentration dependence of the TRY films was investigated by immersing them in 75 mL of PBS solution with a TRY concentration ranging from 0.25 to 10 nM.

LSZ, OVA, and BSA were prepared as interfering proteins to determine the selective TRY adsorption capacity of the MIP sensor. The selectivity tests were performed with 75 mL of PBS solution (pH 7.4), including the same 10 nM concentration of each protein (TRY (0.24 µg/mL), LSZ (0.143 µg/mL), OVA (0.445 µg/mL), and BSA (0.665 µg/mL)) for 30 min. All TRY adsorption experiments were conducted at room temperature.

To quantify the binding capacities of films, the resonant frequency change (Δf , Hz) was converted to mass via the Sauerbrey equation [27], as follows:

$$\Delta f = -\frac{2f_0^2 \Delta m}{A \sqrt{\mu_q \rho_q}}, \quad (1)$$

where f_0 represents the initial resonant frequency of QCM, Δm represents the change in mass (ng), and A represents the gold surface area of the quartz crystal (0.196 cm²). μ_q and ρ_q represent the density and shear modulus of the QC. Considering the parameters of the 9-MHz AT-cut gold-coated QC for the equation, the frequency change of 1 Hz corresponds to an approximate mass change of 1.07 ng.

3. Results

3.1. Optimized MIP Films

The sensing properties and physical/chemical stabilities of MIP films are greatly influenced by the molar ratios of the template, functional monomer, and crosslinker used for polymerization. Therefore, optimizing the molar ratio of the functional monomer and crosslinker in the MIP precursor solution is necessary to enhance the sensing performance of stable MIP sensors. To determine the optimized sensing behaviors in MIP sensors, various pre-cured polymer films were spin-coated using precursor solutions of EGDMA/MAA with molar ratios of 9:1, 8:2, and 7:3 and a total volume of 10 mM (Figure 1a). As the second step, a constant volume (5 µL) of TRY aqueous solution (0.5 mg/mL) was spread over the films via spin-coating.

After complete photopolymerization and template removal, adsorption tests were conducted in a 75 mL PBS solution (pH 7.4) containing 0.24 µg/mL (10 nM) TRY; Δf values were recorded after TRY adsorption for 30 min. Based on a common key–lock mechanism [28], the MIP films contained artificial binding sites biomimicking the 3D structure of the TRY template on their surface. As shown in Figure S1, for three MIP films, Δf values decreased with TRY protein adsorption. TRY (pI: 10.1–10.5) has positively charged side chains (e.g., arginine, histidine, and lysine) and rich polar uncharged side chains such as serine, threonine, asparagine, and glutamine and other chains (glycine and proline) in pH 7.4 PBS solution. Therefore, hydrogen bonding interactions occur between the carboxyl groups of the polymer matrix and the hydrophilic groups of TRY. Specifically, the positively charged TRY protein in the pH 7.4 PBS solution electrostatically interacts with negatively charged MAA on the poly(MAA-co-EGDMA) surface, enabling selective recognition of TRY proteins [29]. In particular, the adsorption mass on each MIP sensor highly depends on the number of cavities formed to recognize TRY proteins, which are determined by the MAA ratio in the MIP precursor solution. The Δf values decreased from –177 to –306 Hz when the MAA ratio was three. In contrast, the NIP films showed a negligible change in Δf regardless of the MAA ratio because of the nonspecific binding of the TRY proteins on the surface. The equilibrium binding capacities (Q_e) of the MIP and NIP sensors were calculated using the adsorbed mass of TRY proteins on the imprinted poly(MAA-co-EGDMA) films (Figure 1b). With an increase in MAA ratio, the Q_e value of the film gradually increased. Furthermore, based on the molar ratio in two components (EGDMA and MAA), the imprinting factor (IF) was calculated using the equation $IF = Q_{e(\text{MIP})}/Q_{e(\text{NIP})}$. The IF value of each imprinted film was 4.40 (9:1), 4.46 (8:2), and 4.94 (7:3), indicating that the imprinting efficiency increased with increasing MAA content. Moreover, high reusability is important in MIP-based chemosensors for TRY detection to identify the stability and reproducibility of the MIP films. Using the same sensor, an

adsorption–extraction pair process was sequentially repeated five times to investigate the recovery percentage after each use (Figure 1c). When the molar ratio of EGDMA to MAA was 7:3, the recovery percentage continuously decreased because of severe damage to the MIP film by the relatively low crosslinking density during the extraction using a strongly acidic solution. Thus, this MIP film (7:3) was unsuitable for a reusable sensing platform even though it had the highest sensing performance. Alternatively, the other two MIP films exhibited highly rational recovery ($97\% \pm 1.9\%$ for 9:1 and $97\% \pm 2.5\%$ for 8:2) despite continuous reuse.

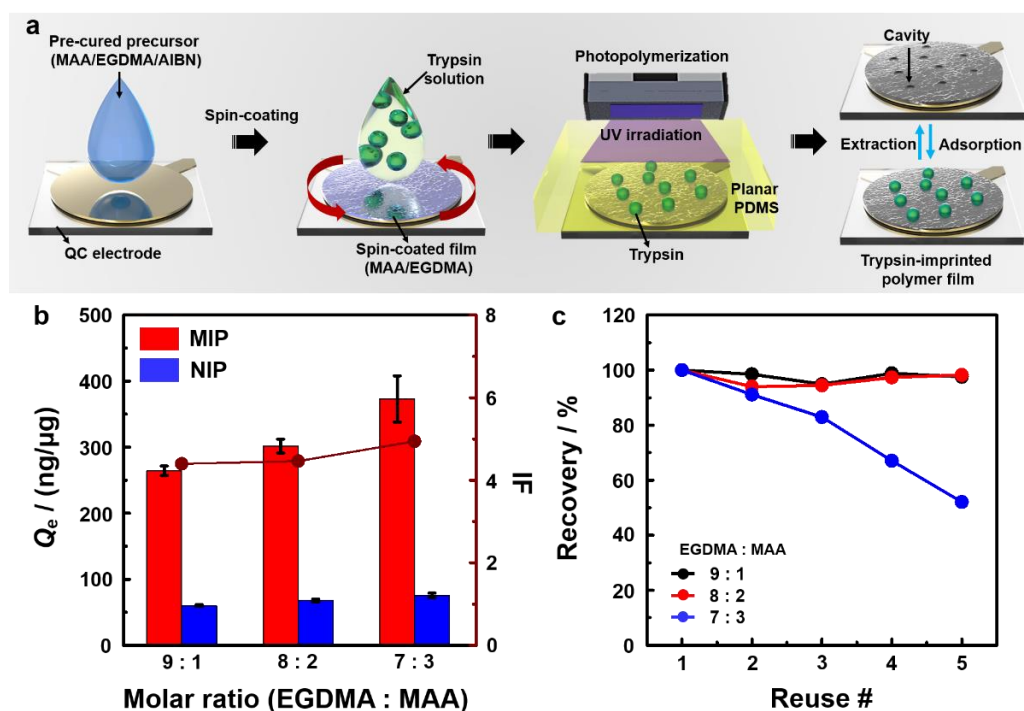


Figure 1. (a) Schematic diagram of the molecularly imprinted polymer (MIP) fabrication. (b) Adsorption capacity at equilibrium (Q_e) of MIP and nonimprinted polymer (NIP) sensors, prepared with different molar ratios of crosslinker and functional monomer; adsorption for 30 min in a 75 mL phosphate-buffered saline (PBS, 10 mM, pH = 7.4) solution containing 0.24 μ g/mL trypsin (TRY) protein ($n = 3$). (c) Recovery percentage of MIP sensors, prepared with different molar ratios of crosslinker and functional monomer, for each resonant frequency change (Δf) measurement after TRY adsorption (number of reuses, $n = 5$).

For effective template imprinting, surface imprinting with a PDMS mold was performed after spin-coating the TRY solutions (5 μ L each) with various concentrations (0.1–2.0 mg/mL) on the pre-cured polymer films. As shown in the inset of Figure 2a, the surface of spin-coated NIP film is smooth, whereas two MIP films show relatively rough surfaces due to the TRY aggregates. In the sample corresponding to the highest TRY concentration, the TRY aggregates distinctly appear on the surface. The formation of too many aggregates causes a lower sensing response due to the possibility of heterogeneous adsorption. The film thickness of the MIP and NIP films was approximately 200 nm (Figure S2) [30]. After TRY template removal, four imprinted chemosensors were evaluated by measuring Δf after TRY adsorption for 30 min in 75 mL of PBS solution (pH 7.4) containing 0.24 μ g/mL TRY. As shown in Figure 2a, the sensing response of the MIP(0.5) film generated the highest Δf (−210.62 Hz) due to the relatively well-distributed imprinted sites. Excessive TRY loading yielded protein aggregates that caused a low sensing response due to the formation of heterogeneous binding sites. Thus, the efficient MIP(0.5) film optimized from these imprinting conditions (through the control of monomer/crosslinker components and template concentration) was used to investigate all of the sensing properties. To in-

investigate the chemical characteristics of the MIP and NIP films, Fourier-transform infrared (FT-IR) spectra were used, as shown in Figure 2b. The intensive absorption band observed at ca. 1730 cm^{-1} for all poly(MAA-co-EGDMA) films is attributed to C = O stretching vibrations [31]. In addition, the intense absorption peaks corresponding to the C = C stretch ($1636\text{--}1648\text{ cm}^{-1}$) and C–H out-of-plane bend at a double bond (950 cm^{-1}) for all films were observed in the FT-IR spectra. An absorption peak corresponding to N–H bending at 1540 cm^{-1} appeared on the imprinted TRY film [32]. However, this peak disappeared in the TRY-extracted MIP film spectrum, indicating that the imprinted TRY templates were completely removed by extraction.

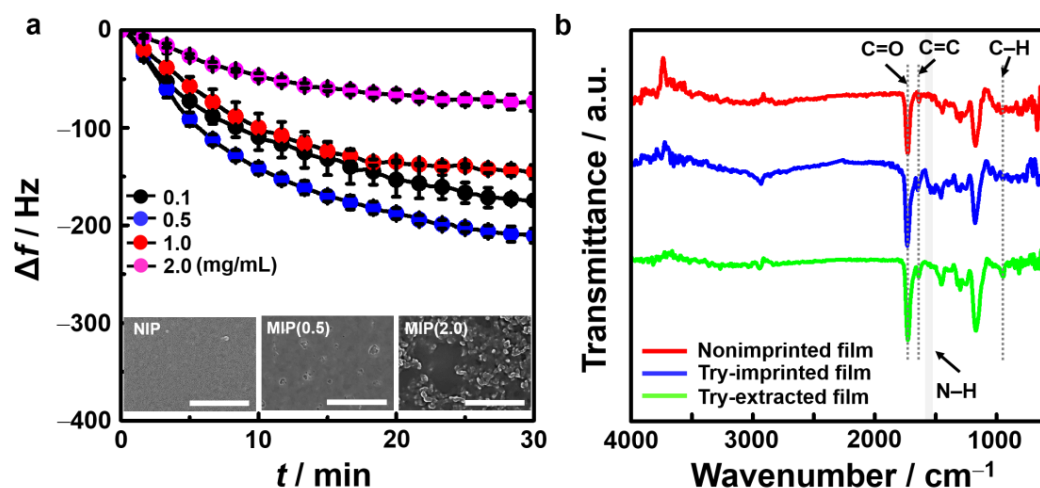


Figure 2. (a) Δf of MIP sensors fabricated by spin-coating solution of different TRY concentrations (0.1–2.0 mg/mL). The measurements were performed in a 75 mL PBS (10 mM, pH = 7.4) solution containing $0.24\text{ }\mu\text{g/mL}$ TRY for 30 min for adsorption. The insets of Figure 2a show SEM images of NIP film and MIP films (MIP(0.5) and MIP(2.0) made by spin-coating with 0.5 and 2.0 mg/mL TRY solutions, respectively). All scale bars are $1\text{ }\mu\text{m}$. (b) Fourier-transform infrared spectra of NIP and TRY-imprinted/extracted MIP films.

3.2. Sensing Properties

The sensing behaviors of MIP and NIP films on gold-coated QCs were evaluated by measuring the Δf of the sensors in a 75 mL PBS solution (pH 7.4) having a TRY concentration of $0.006\text{--}0.24\text{ }\mu\text{g/mL}$ ($0.25\text{--}10\text{ nM}$) for 30 min (Figure 3a,b). When the TRY solution was concentrated, the Δf value dramatically decreased for the MIP film from -31 to -210 Hz . The functional MAA monomer in the TRY-extracted cavities of the MIP films was non-covalently bonded to the side chains of TRY via hydrogen bonding during the adsorption. However, the NIP film exhibited only a 20 Hz decrease in Δf from -27 to -47 Hz under the same solution conditions as the MIP film was employed for TRY adsorption, due to nonspecific adsorption onto the surface of the NIP film without the imprinted cavities. For the MIP film, the sensitivity ($-841 \pm 65\text{ Hz}/(\mu\text{g/mL})$) with a coefficient of determination (R^2) of 0.970 was approximately 11-fold higher than the NIP film ($-79 \pm 8\text{ Hz}/(\mu\text{g/mL})$) with an R^2 of 0.95 (Figure S3). The adsorption capacity at equilibrium (Q_e), calculated from the Δf value of TRY adsorption, was replotted as a function of TRY concentration. Figure S4 shows the IF value as a function of TRY concentration, calculated based on the adsorbed TRY mass per poly(MAA-co-EGDMA) unit weight (i.e., $Q_{\text{MIP}}/Q_{\text{NIP}}$) [33]. The IF value of the MIP film was exponentially increased up to 4.5 within the examined concentration range. From these results, the LOD and LOQ of the TRY-imprinted sensors were calculated by linear calibration curves at the lower range of concentrations, from $0.006\text{ }\mu\text{g/mL}$ to $0.06\text{ }\mu\text{g/mL}$, as seen in Figure 3c. Furthermore, the LOD and LOQ of the MIP and NIP films were calculated using linear regression equations. The equations of the LOD and LOQ are $k \times (S/m)$, where S is the standard deviation of the y -intercept and m equals the slope of the calibration curve, with $k = 3$ for the LOD and 10 for the LOQ. The LOD and

LOQ values of the MIP film were 25.33 and 84.42 ng/mL, respectively. However, those in the NIP film had relatively higher values (LOD and LOQ of 40.55 and 135.15 ng/mL, respectively). Table 1 shows the performance comparison such as the concentration range, the LOD, and the IF (for MIP) of the reported QCM sensors for the detection of TRY.

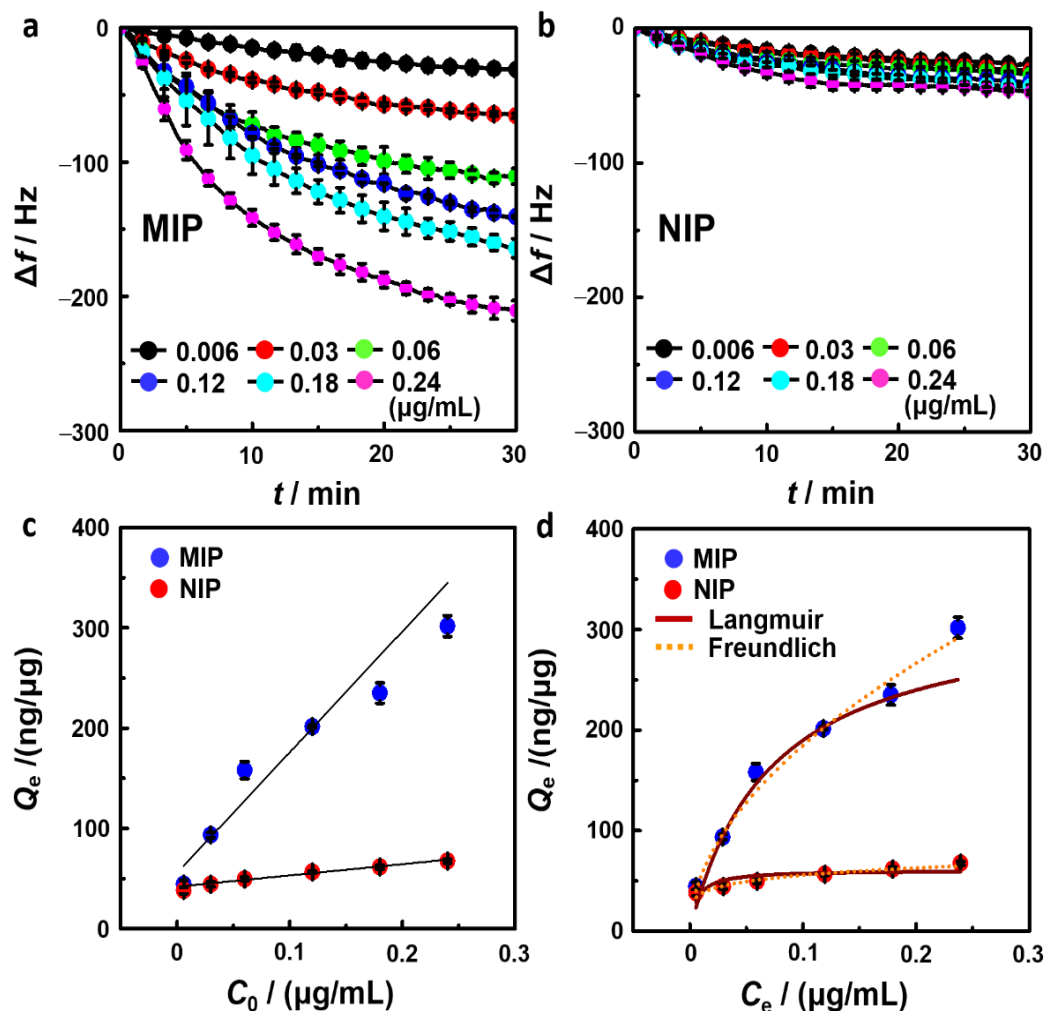


Figure 3. (a,b) Δf as a function of time for (a) MIP and (b) NIP film-coated quartz crystal microbalance (QCM) sensors in a 75 mL PBS (10 mM, pH = 7.4) solution containing TRY concentration ranging from 0.006 to 0.24 $\mu\text{g/mL}$ during the adsorption. (c) Q_e values as a function of TRY concentration (C_0) for the MIP/NIP film-coated QCM sensors. The measurements were performed individually in a 75 mL PBS (10 mM, pH = 7.4) solution containing TRY with concentrations ranging from 0.006 μg to 0.240 $\mu\text{g/mL}$. (d) Q_e values of MIP and NIP films as a function of the equilibrium concentration of TRY after adsorption. The Langmuir isotherm and Freundlich isotherm models were fitted for both films.

Table 1. Comparison of evaluation parameters (LOD, LOQ, and IF) for QCM sensors.

Sensor Configuration	Preparation Method	Concentration Range ($\mu\text{g/mL}$)	LOD (ng/mL)	IF	Reference
Poly(MAA-co-EGDMA) MIP particles	Mini emulsion polymerization	0.125–2	70	<3.5	[10]
Poly(AA-co-EGDMA) MIP film	Thermal polymerization	10–100	100	–	[20]
Poly(<i>o</i> -PD) MIP film	Electropolymerization	0.24–48	70.9	3.51	[21]
TI-Cys-GA	Self-assembly	25–125	3800	–	[34]
Au NP-MCA-Peptide	Self-assembly	0–0.75	8.6	–	[35]
Poly(MAA-co-EGDMA) MIP film	Photopolymerization and spin-coating	0.006–0.24	25.33	<4.5	This work

MIP: molecularly imprinted polymer; MAA: methacrylic acid; EGDMA: ethylene glycol dimethacrylate; AA: acrylic acid; *o*-PD: *o*-phenylenediamine; TI: trypsin inhibitor; Cys: cysteamine; GA: glutaraldehyde; NP: nanoparticle; MCA: mercaptoacetic acid.

Moreover, TRY adsorption behaviors on the MIP/NIP films were evaluated using adsorption isotherm models. Figure 3d shows the Q_e values as a function of the C_e and they were calculated from the Δf values after TRY adsorption on both MIP/NIP films. The real data points were fitted using two typical adsorption isotherm models: Langmuir and Freundlich. The Langmuir isotherm assumes that the adsorption occurs on a monolayer containing a finite number of homogeneous adsorption sites. Conversely, the Freundlich isotherm assumes that the adsorption occurs on multilayers containing heterogeneous adsorption sites. The Langmuir and Freundlich models are described in Equations (2) and (3), respectively [36,37]:

$$Q_e = \frac{K_L Q_m C_e}{1 + K_L C_e}, \quad (2)$$

$$Q_e = K_F C_e^{\frac{1}{n}}, \quad (3)$$

where Q_m is the maximum adsorption capacity, K_L is the adsorption equilibrium constant for Langmuir, K_F is the adsorption equilibrium constant for Freundlich, and $1/n$ is the surface heterogeneity. The isotherm parameters in the nonlinear fitting curve are summarized in Table 2. Based on the evaluation of the R^2 values of the two models, the MIP/NIP films were better fitted to the Freundlich model than to the Langmuir model. From the result, it was found that the preferential heterogeneous adsorption in the multimolecular layers occurred on the surface of the MIP/NIP films.

Table 2. Adsorption isotherm parameters of Langmuir and Freundlich models in the MIP/NIP films.

Sensors	Langmuir			Freundlich		
	K_L (mL/ μ g)	Q_m (ng/ μ g)	R^2	K_F	$1/n$	R^2
MIP	14.01	325.42	0.976	623.51	0.528	0.995
NIP	163.51	60.97	0.494	83.22	0.174	0.942

To evaluate the selectivity of the MIP/NIP sensors, the Δf values were measured in individual PBS solutions (75 mL, pH 7.4) with 0.24 μ g/mL of TRY or interfering proteins (LSZ, OVA, or BSA) during 30 min of adsorption (Figure 4a and Figure S5). Depending on the imprinted efficiency, the TRY sensing response was significantly higher than that of the other proteins. In addition, relatively lower Δf values between 31 and 54 appeared for the other proteins due to nonspecific adsorption owing to the TRY structural similarity to the target protein, including minor effects such as pI value and molecular weight. In NIP film, nonimprinted TRY resulted in a highly inadequate sensing response regardless of the protein type because of nonspecific adsorption. In interference testing, the sensing signal of the MIP sensor was recovered up to approximately 95.3%, compared to the signal for TRY, indicating that the MIP film exhibited high accuracy in the protein mixture due to the preferential binding of TRY on the cavities. Moreover, the signal value of the NIP sensor increased more than that in the individual protein because of the increased nonspecific binding in a more concentrated solution. Based on the Δf values obtained from Figure 4a, the Q_e values were calculated for each protein (Figure 4b). For MIP film, the selectivity coefficient (k^*), defined as Q_e (TRY)/ Q_e (interfering protein), was 3.90 for LSZ, 5.40 for OVA, and 6.78 for BSA, compared to those of NIP film ($k^* = 1.24$ – 2.64). Thus, this surface imprinting through a simple spin-coating method provided sufficient imprinted sites and selective spatial structure for protein recognition and selection on the MIP film.

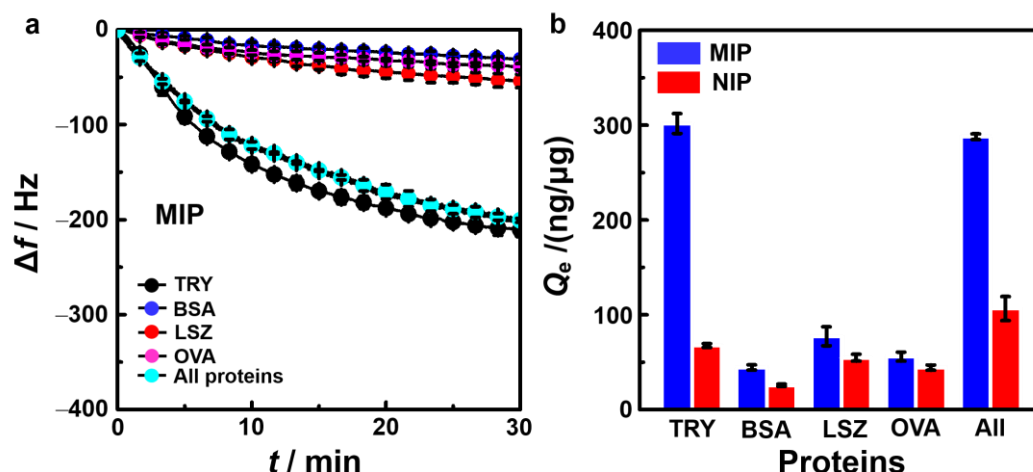


Figure 4. (a) Δf as a function of time during the adsorption of TRY and interfering proteins. (b) Q_e values of MIP/NIP film-coated QCM sensors for different proteins (TRY, bovine serum albumin (BSA), lysozyme (LSZ), and ovalbumin (OVA)). All of the measurements were carried out in a 75 mL PBS (10 mM, pH = 7.4) solution containing 0.24 μ g/mL of individual proteins or all proteins (total concentration = 0.96 μ g/mL).

4. Conclusions

In this study, TRY-surface-imprinted polymer films were successfully fabricated on a gold-coated QC substrate via two-step spin-coating and sequential photopolymerization. The composition of MAA and EGDMA in the precursor solution and the concentration of TRY in the imprinting solution were optimized to design efficient MIP films with maximum TRY adsorption capacity. Sensing properties, including binding capacity, sensitivity, and selectivity, of the TRY-imprinted sensors were evaluated by measuring the Δf values of QCM during the adsorption. The MIP film showed a high IF (4.5) in a PBS solution (pH 7.4) containing TRY at a concentration of 0.24 μ g/mL, and the LOD was calculated to be 25.33 ng/mL. Moreover, the k^* value of the MIP film showed a significant increase against TRY over other proteins. In contrast, the NIP film had relatively low selectivity due to the nonspecific adsorption for all proteins. Therefore, the simple and rapid protein-surface-imprinting method using spin-coating and photopolymerization could provide high sensitivity and selectivity to develop TRY chemosensors by efficiently generating recognizable cavities in the MIP matrix.

Supplementary Materials: The following supporting information can be downloaded at: <https://www.mdpi.com/article/10.3390/chemosensors11030189/s1>, Figure S1—Frequency change as a function of time on the MIP/NIP films; Figure S2—Cross-sectional SEM images of the MIP/NIP films; Figure S3—Frequency change as a function of TRY concentration on the MIP/NIP films; Figure S4—Imprinting factor as a function of TRY concentration; Figure S5—Frequency change with various proteins as a function of time on the MIP/NIP films.

Author Contributions: Investigation, J.W.B., J.C.Y. and S.J.L.; methodology, J.W.B., J.C.Y. and C.H.C.; supervision, J.P.P. and J.P.; writing—original draft, J.P.P. and J.P. All authors have read and agreed to the published version of the manuscript.

Funding: This work was supported by the Basic Science Research Program through the National Research Foundation of Korea (NRF) by the Ministry of Education (NRF-2020R111A3070148).

Institutional Review Board Statement: Not applicable.

Informed Consent Statement: Not applicable.

Data Availability Statement: Not applicable.

Conflicts of Interest: The authors declare no conflict of interest.

References

1. Mótóyán, J.A.; Tóth, F.; Tőzsér, J. Research applications of proteolytic enzymes in molecular biology. *Biomolecules* **2013**, *3*, 923–942. [[CrossRef](#)]
2. Shah, D.; Mital, K. The role of trypsin: Chymotrypsin in tissue repair. *Adv. Ther.* **2018**, *35*, 31–42. [[CrossRef](#)]
3. Logsdon, C. Phosphatidylinositol 3-kinase and trypsin activation in pancreatitis. *J. Clin. Investig.* **2001**, *108*, 1267–1268. [[CrossRef](#)]
4. Ko, J.; Cho, J.; Petrov, M.S. Low serum amylase, lipase, and trypsin as biomarkers of metabolic disorders: A systematic review and meta-analysis. *Diabetes Res. Clin. Pract.* **2020**, *159*, 107974. [[CrossRef](#)]
5. Yi, Q.; Liu, Q.; Gao, F.; Chen, Q.; Wang, G. Application of an electrochemical immunosensor with a MWCNT/PDAA modified electrode for detection of serum trypsin. *Sensors* **2014**, *14*, 10203–10212. [[CrossRef](#)]
6. Weiss, F.U. Pancreatic cancer risk in hereditary pancreatitis. *Front. Physiol.* **2014**, *5*, 70. [[CrossRef](#)]
7. Fonseca, V.; Epstein, O.; Katrak, A.; Junglee, D.; Mikhailidis, D.P.; McIntyre, N.; Dandona, P. Serum immunoreactive trypsin and pancreatic lipase in primary biliary cirrhosis. *J. Clin. Pathol.* **1986**, *39*, 638–640. [[CrossRef](#)] [[PubMed](#)]
8. Kong, W.; Li, Q.; Xia, L.; Li, X.; Sun, H.; Kong, R.M.; Qu, F. Photoelectrochemical determination of trypsin by using an indium tin oxide electrode modified with a composite prepared from MoS₂ nanosheets and TiO₂ nanorods. *Microchim. Acta* **2019**, *186*, 490. [[CrossRef](#)]
9. Zhang, L.; Du, J. A sensitive and label-free trypsin colorimetric sensor with cytochrome c as a substrate. *Biosens. Bioelectron.* **2016**, *79*, 347–352. [[CrossRef](#)] [[PubMed](#)]
10. Karaseva, N.A.; Pluhar, B.; Beliaeva, E.A.; Ermolaeva, T.N.; Mizaikoff, B. Synthesis and application of molecularly imprinted polymers for trypsin piezoelectric sensors. *Sens. Actuators B Chem.* **2019**, *280*, 272–279. [[CrossRef](#)]
11. Braatz, J.A.; Elias, C.; Finny, J.G.; Tran, H.; McCaman, M. Quantitation of residual trypsin in cell-based therapeutics using immobilized α -1-antitrypsin or SBTI in an ELISA format. *J. Immunol. Methods* **2015**, *417*, 131–133. [[CrossRef](#)]
12. BelBruno, J.J. Molecularly imprinted polymers. *Chem. Rev.* **2019**, *119*, 94–119. [[CrossRef](#)]
13. Bossi, A.; Bonini, F.; Turner, A.P.F.; Piletsky, S.A. Molecularly imprinted polymers for the recognition of proteins: The state of the art. *Biosens. Bioelectron.* **2007**, *22*, 1131–1137. [[CrossRef](#)]
14. Bognár, Z.; Supala, E.; Yarman, A.; Zhang, X.; Bier, F.F.; Scheller, F.W.; Gyurcsányi, R.E. Peptide epitope-imprinted polymer microarrays for selective protein recognition. Application for SARS-CoV-2 RBD protein. *Chem. Sci.* **2022**, *13*, 1263–1269. [[CrossRef](#)] [[PubMed](#)]
15. Bartold, K.; Iskierko, Z.; Borowicz, P.; Noworyta, K.; Lin, C.Y.; Kalecki, J.; Sharma, P.S.; Lin, H.Y.; Kutner, W. Molecularly imprinted polymer-based extended-gate field-effect transistor (EG-FET) chemosensor for selective determination of matrix metalloproteinase-1 (MMP-1) protein. *Biosens. Bioelectron.* **2022**, *208*, 114203. [[CrossRef](#)] [[PubMed](#)]
16. Guo, Z.; Sun, Y.; Zhang, L.; Ding, Q.; Chen, W.; Yu, H.; Liu, Q.; Fu, M. Surface imprinted core-shell nanorod for selective extraction of glycoprotein. *J. Colloid Interface Sci.* **2022**, *615*, 597–605. [[CrossRef](#)]
17. Luo, Y.; Bai, C.C.; Liu, M.X.; Wang, D.; Chen, M.Y.; Yu, S.S.; Bu, X.Y.; Wang, X.H. PEGylation of boronate-affinity-oriented surface imprinting magnetic nanoparticles with improved performance. *Talanta* **2022**, *238*, 122992. [[CrossRef](#)]
18. Liu, Z.; Yin, Z.Z.; Cai, W.R.; Wu, D.; Li, J.; Kong, Y. A surface protein-imprinted biosensor based on boronate affinity for the detection of anti-human immunoglobulin G. *Microchim. Acta* **2022**, *189*, 106. [[CrossRef](#)]
19. Kanubaddi, K.R.; Huang, P.Y.; Chang, Y.L.; Wu, C.H.; Li, W.; Kankala, R.K.; Tai, D.F.; Lee, C.H. Deviation of Trypsin Activity Using Peptide Conformational Imprints. *Nanomaterials* **2021**, *11*, 334. [[CrossRef](#)]
20. Hayden, O.; Haderspöck, C.; Krassnig, S.; Chen, X.; Dickert, F.L. Surface imprinting strategies for the detection of Trypsin. *Analyst* **2006**, *131*, 1044–1050. [[CrossRef](#)] [[PubMed](#)]
21. Choi, D.Y.; Yang, J.C.; Park, J. Optimization and characterization of electrochemical protein imprinting on hemispherical porous gold patterns for the detection of trypsin. *Sens. Actuators B Chem.* **2022**, *350*, 130855. [[CrossRef](#)]
22. Kalecki, J.; Iskierko, Z.; Cieplak, M.; Sharma, P.S. Oriented immobilization of protein templates: A new trend in surface imprinting. *ACS Sens.* **2020**, *5*, 3710–3720. [[CrossRef](#)] [[PubMed](#)]
23. Tan, C.J.; Tong, Y.W. Molecularly imprinted beads by surface imprinting. *Anal. Bioanal. Chem.* **2007**, *389*, 369–376. [[CrossRef](#)] [[PubMed](#)]
24. Schmidt, R.H.; Mosbach, K.; Haupt, K. A simple method for spin-coating molecularly imprinted polymer films of controlled thickness and porosity. *Adv. Mater.* **2004**, *16*, 719–722. [[CrossRef](#)]
25. Toolan, D.T.W.; Howse, J.R. Development of in situ studies of spin coated polymer films. *J. Mater. Chem. C* **2013**, *1*, 603–616. [[CrossRef](#)]
26. Hawkins, D.M.; Stevenson, D.; Reddy, S.M. Investigation of protein imprinting in hydrogel-based molecularly imprinted polymers (HydroMIPs). *Anal. Chim. Acta* **2005**, *542*, 61–65. [[CrossRef](#)]
27. Lowdon, J.W.; Diliën, H.; Singla, P.; Peeters, M.; Cleij, T.J.; van Grinsven, V.; Eersels, K. MIPs for commercial application in low-cost sensors and assays—An overview of the current status quo. *Sens. Actuators B Chem.* **2020**, *325*, 128973. [[CrossRef](#)]
28. Akgönüllü, S.; Kılıç, S.; Esen, C.; Denizli, A. Molecularly imprinted polymer-based sensors for protein detection. *Polymers* **2023**, *15*, 629. [[CrossRef](#)]
29. Bunina, Z.Y.; Bryleva, K.; Yurchenko, O.; Belikov, K. Sorption materials based on ethylene glycol dimethacrylate and methacrylic acid copolymers for rare earth elements extraction from aqueous solutions. *Adsorp. Sci. Technol.* **2017**, *35*, 545–559. [[CrossRef](#)]

30. Qin, D.; Wang, L.; Wang, Y.; Du, X.; Zhang, L.; Zhang, Q.; He, B. Shape-controlled synthesis of protein-conjugated CdS nanocrystals (NCs) and study on the binding of Cd²⁺/CdS to trypsin. *J. Nanopart. Res.* **2017**, *19*, 252. [[CrossRef](#)]
31. Gryshchenko, A.O.; Bottaro, C.S. Development of molecularly imprinted polymer in porous film format for binding of phenol and alkylphenols from water. *Int. J. Mol. Sci.* **2014**, *15*, 1338–1357. [[CrossRef](#)]
32. Poole, S.; West, S.I.; Walters, C.L. Protein–protein interactions: Their importance in the foaming of heterogeneous protein systems. *J. Sci. Food Agric.* **1984**, *35*, 701–711. [[CrossRef](#)]
33. Tyona, M.D. A theoretical study on spin coating technique. *Adv. Mater. Res.* **2013**, *2*, 195–208. [[CrossRef](#)]
34. Huang, Y.Y.; Zhang, Q.D.; Liu, G.O.; Zhao, R. A continuous-flow mass biosensor for the real-time dynamic analysis of protease inhibition. *Chem. Commun.* **2015**, *51*, 6601–6604. [[CrossRef](#)]
35. Dong, Z.M.; Cheng, L.; Zhang, P.; Zhao, G.C. Label-free analytical performances of a peptide-based QCM biosensor for trypsin. *Analyst* **2020**, *145*, 3329–3338. [[CrossRef](#)] [[PubMed](#)]
36. Li, Z.; Yang, Y.; Jauregui-Haza, U.; Guo, Z.; Campos, L.C. Investigation of metaldehyde removal by powdered activated carbon from different water samples. *Environ. Sci. Water Res. Technol.* **2020**, *6*, 1432–1444. [[CrossRef](#)]
37. Li, X.; Liu, H.; Deng, Z.; Chen, W.; Li, T.; Zhang, Y.; Zhang, Z.; He, Y.; Tan, Z.; Zhong, S. PEGylated thermo-sensitive bionic magnetic core-shell structure molecularly imprinted polymers based on halloysite nanotubes for specific adsorption and separation of bovine serum albumin. *Polymers* **2020**, *12*, 536. [[CrossRef](#)]

Disclaimer/Publisher’s Note: The statements, opinions and data contained in all publications are solely those of the individual author(s) and contributor(s) and not of MDPI and/or the editor(s). MDPI and/or the editor(s) disclaim responsibility for any injury to people or property resulting from any ideas, methods, instructions or products referred to in the content.